# Contents

# List of Figures



# List of Tables

# 1. Abstract

The halogen iodine exists mainly as a diatomic Molecule $I_2$ which exhibits excellent properties for spectroscopy. There is only one naturally occurring stable isotope of iodine which rules out any mixture of different spectra. The first part of the experiment consists of measuring the absorption spectrum of the $I_2$ molecule with a CCD spectrometer. Almost all of the measured values contain the literature value in the margin of a single standard deviation. We calculated the values, shown in Table 1.1.

Table 1.1.: Results of the experiment

| $n''$ | $\omega'_e$ | $\omega'_e x'_e$ | $D_{e,morse}$ | $D_e$ |
|---|---|---|---|---|
| 0 | $126 \pm 26\,\mathrm{cm}^{-1}$ | $0.9 \pm 0.5\,\mathrm{cm}^{-1}$ | $4400 \pm 3000\,\mathrm{cm}^{-1}$ | $4400 \pm 2700\,\mathrm{cm}^{-1}$ |
| 1 | $111 \pm 15\,\mathrm{cm}^{-1}$ | $0.6 \pm 0.3\,\mathrm{cm}^{-1}$ | $5200 \pm 2900\,\mathrm{cm}^{-1}$ | $5200 \pm 2800\,\mathrm{cm}^{-1}$ |
| 2 | $125 \pm 17\,\mathrm{cm}^{-1}$ | $0.8 \pm 0.4\,\mathrm{cm}^{-1}$ | $4900 \pm 2900\,\mathrm{cm}^{-1}$ | $4900 \pm 2600\,\mathrm{cm}^{-1}$ |

The excitation energy $T'_e = 15\,900 \pm 300\,\mathrm{cm}^{-1}$ and $E_{diss} = 20\,200 \pm 2700\,\mathrm{cm}^{-1}$ were calculated for the progression of $n'' = 0$. For different possible reasons, we were not able to properly perform the emission part of the experiment, which is why we analysed the absorption bands in more detail.

# 2. Theoretical Foundations

## 2.1. Vibrations

### 2.1.1. Vibrational energies of molecules

Classically the energy of a diatomic molecule can be described by expressing it through the potential of an harmonic oscillator. The energies and frequencies of the different states are than easily deductible.

### 2.1.2. Morse potential

The Morse potential (2.1) is an approximative description to explain the potential of vibronic states of a molecule. The main advantage of the Morse potential consists in being able to deliver exact solutions for the Schrödinger equation. The Introduction of the Morse potential is necessary because the oscillations of the electrons do not remain harmonic at large displacements for the equilibrium position.

$$V(x) = D_e(1 - e^{-a(r-r_e)})^2 \tag{2.1}$$

Here $D_e$ is the dissociation of the molecule, $r_e$ is the distance between the nuclei. The parameter 'a' is a molecule constant. Putting the Morse potential into the Schrödinger equation will give you the following solutions:

$$E_n = (n + \frac{1}{2})\ \hbar\omega_e - (n + \frac{1}{2})^2\ \hbar\omega_e x_e \tag{2.2}$$

$$\text{with :} \tag{2.3}$$

$$\omega_e = a\sqrt{\frac{\hbar D_e}{\pi c \mu}} \tag{2.4}$$

$$\omega_e x_e = \frac{a^2\hbar}{\mu 4\pi c}. \tag{2.5}$$

The $\mu$ represents the reduced atomic mass which is calculated through $\mu = \frac{m_e m_c}{m_e + m_c}$.
By comparing this solution to the solution of the harmonic oscillator one sees, that the term containing $\omega_e x_e$ is the anharmonic factor, which makes $\omega_e x_e$ the anharmonic constant. This term accounts for the anharmonic behaviour of the electronic potential at higher quantum numbers n as seen in figure 2.1. In this Graph one can see that even though the Morse potential is not a good approximation for $R < R_e$ it matches closely for $R \geq R_e$

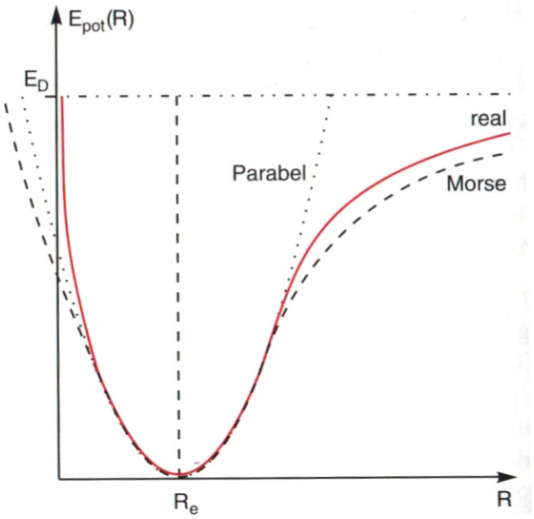


Figure 2.1.: Comparison of the Morse potential to the real potential of the electrons [Mey, 12]

Using the the equations (2.4) and (2.5) the dissociation energy is given by :

$$D_e = \frac{\omega_e^2}{4\omega_e x_e} \tag{2.6}$$

### 2.1.3. Birge-Sponer plot

By using perturbation theory on the harmonic potential we get (from [Mey, 9]):

$$G(n) = (n + \frac{1}{2})\ \hbar\omega_e - (n + \frac{1}{2})^2\ \hbar\omega_e x_e + (n + \frac{1}{3})^3 \hbar\omega_e y_e ... \tag{2.7}$$

Using (2.7) the energy difference between two different states is given with:

$$\Delta G(n + \frac{1}{2}) = G(n + 1) - G(n) = \omega_e - \omega_e x_e(2n + 2) + \omega_e y_e(3n^2 + 6n + \frac{13}{4}) + ... \tag{2.8}$$

The Birge-Sponer plot consist of $\Delta G(n + \frac{1}{2})$ being plotted over $n + \frac{1}{2}$.
By examining the electronic potential, one can see that there must be a finite maximal $n_{diss}$ which forms the border between the diatomic molecule and its dissociation. Therefore we know that:

$$\Delta G(n_{diss} + \frac{1}{2}) = 0. \tag{2.9}$$

Using this we can determine the dissociation energy of the ground state n = 0 as:

$$D_e(0) = \sum_{n=0}^{n_{diss}} \Delta G(n + \frac{1}{2}) \tag{2.10}$$

## 2.2. Electronic Transitions

The electronic configuration of the J2 molecule in it's ground state is given by :

$$... (\sigma_g 5s)^2\ (\sigma_\mu^* 5s)^2\ (\sigma_g 5p)^2\ (\pi_u 5p)^4\ (\pi_g^* 5p)^4$$

the electronic configuration for the first excited state is described through:

$$... (\sigma_g 5s)^2\ (\sigma_\mu^* 5s)^2\ (\sigma_g 5p)^2\ (\pi_u 5p)^4\ (\pi_g^* 5p)^3\ (\sigma_\mu^* 5p).$$

### 2.2.1. Notation

In this experiment we are going to observe the following transition:

$$X^1\Sigma_g^+ \leftrightarrow B^3\Pi_u^+$$

Here the capital X stands for the ground- and the capital B for the second exited state. The number on the upper left of the Greek letter is referred to as the multiplicity of the molecule. It is given through 2S+1 where S is the total spin of the molecule. A multiplicity of 1 indicates a singlet whereas a multiplicity of 3 indicates a triplet.
The capital Greek letters represent the total angular momentums of the molecule. Their values are calculated using LCAO and are having the following values of $\Lambda$:

$$\Lambda = 0, 1, 2, 3, 4, ... \leftrightarrow \Sigma, \Pi, \Delta, \Phi ...$$

The signs on the upper right indicates the effect reflection. Last but not least the letter on the lower right indicates the parity of the molecular orbitals. Those describe the behaviour of the orbitals under the inversion of the electron coordinates. If the orbitals remain unchanged they are even and notified with a g. If the orbitals however change their sign, they are uneven and notified with a u.

### 2.2.2. Energy differences

The transition of the molecule from one state to the other is due to the absorption or emission of a Photon with an Energy that is matching the energy difference of the two states. The transition of molecule from one state to an other can be observed trough a change of the vibrational state of the molecule. This means that the molecule will change its vibration frequency which in return can be observed in the absorption spectrum.
Apart from vibronic transitions there are also rotational transitions. These are less energetic and will not be observed in our experiment. One can see the difference between the two transitions in graph 2.2 .

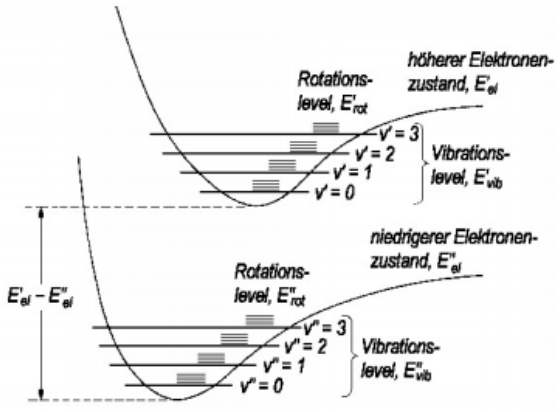


Figure 2.2.: structure of the different states [Mey, 16]

The energy difference of the two vibrational states ,wich is the engergy of the transition, is given by:

$$\Delta G = G'(n') - G''(n'') + T_e = \omega_e'(n' + \frac{1}{2}) - \omega_e''(n'' + \frac{1}{2}) - \omega_e' x_e'(n' + \frac{1}{2})^2 + \omega_e'' x_e''(n'' + \frac{1}{2})^2 + T_e$$

$T_e$ stands for the excitation energy of the molecule.

### 2.2.3. Selection Rules

To determine the selection rules for the different electronic transitions for diatomic molecules we will have to use the following parameter:

$$\Omega = \Lambda + \Sigma.$$

The selection rules are as follows:

- g $\leftrightarrow$ u , g $\nleftrightarrow$ g , u $\nleftrightarrow$ u
- $\Sigma^{+/-} \leftrightarrow \Sigma^{+/-}$ , $\Sigma^{+/-} \nleftrightarrow \Sigma^{-/+}$
- $\Delta\Lambda = 0, \pm 1$
- $\Delta\Omega = 0, \pm 1$
- $\Delta S = 0$

## 2.3. Bernd-Oppenheimer Approximation

The Bernd-Oppenheimer approximation states that since the difference in mass between the nuclei and the electrons are very significant, the movement of the nuclei is not influenced by the movement of the orbital electrons. As a consequence one can write the wave function of the atom as a product of the wave function of the core ($R_i$) and the wave function of the electron ($r_i$) as seen in 2.11 . This is a useful tool for solving the Schrödinger-equation, because in using this approximation one can see the core as static and solve the equation only for the electrons.

$$\Psi_{r_i,R_i} = \psi(r_i, R_i)\chi(R_i) \tag{2.11}$$

## 2.4. Franck-Condon Principle

As the mass of an electron is far smaller than the mass of the atomic core, the nuclei does not move during an electronic transition. It only moves after the Electron has reached it's new state. As a consequence we can observe in figure 2.3 that the electronic transitions are represented by a straight line.

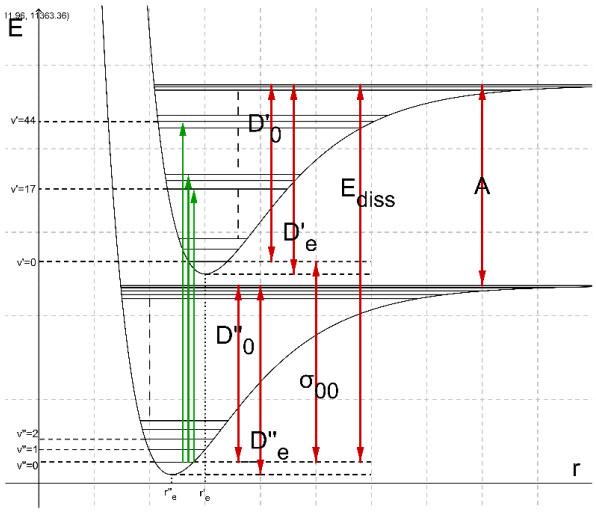


Figure 2.3.: Electronic transition in relation to internuclear distances [Mey, 23]

Furthermore the principle states that the probability of a transition from one vibronic state to an other is directly correlated to the similarity of the electronic wave functions of the two states. The more these wave functions reassemble one an other, the higher the probability of a transition. The relative intensities of these transitions are expressed trough the Franck-Condon factor (2.12)

$$FC(v_i', v_k'') = \left| \int \Psi'_v \Psi''_v dr \right|^2 \tag{2.12}$$

# 3. Experimental setup

## 3.1. Absorption

For the first part of the experiment a halogen lamp with a continuous spectrum is fixed on an optical bench and mirrors are used to guide the beam of light through a tube filled with iodine, which is heated through an internal heater and an external hair dryer, onto a USB3000 spectrometer. The spectrometer is connected to a computer to process the data. With the use of two lenses, one before the tube and one behind it, the intensity of the light arriving at the spectrometer is maximized. The setup can be seen in figure 3.1.

## 3.2. Emission

For the second part of the experiment, the halogen lamp was replaced with a mercury-vapour lamp which has a discrete spectrum. The USB300 is replaced by a monochromator, which is connected to a photomultiplier and then to a computer as well. After the calibration of the monochromator, the lamp is replaced by a He-Ne laser.

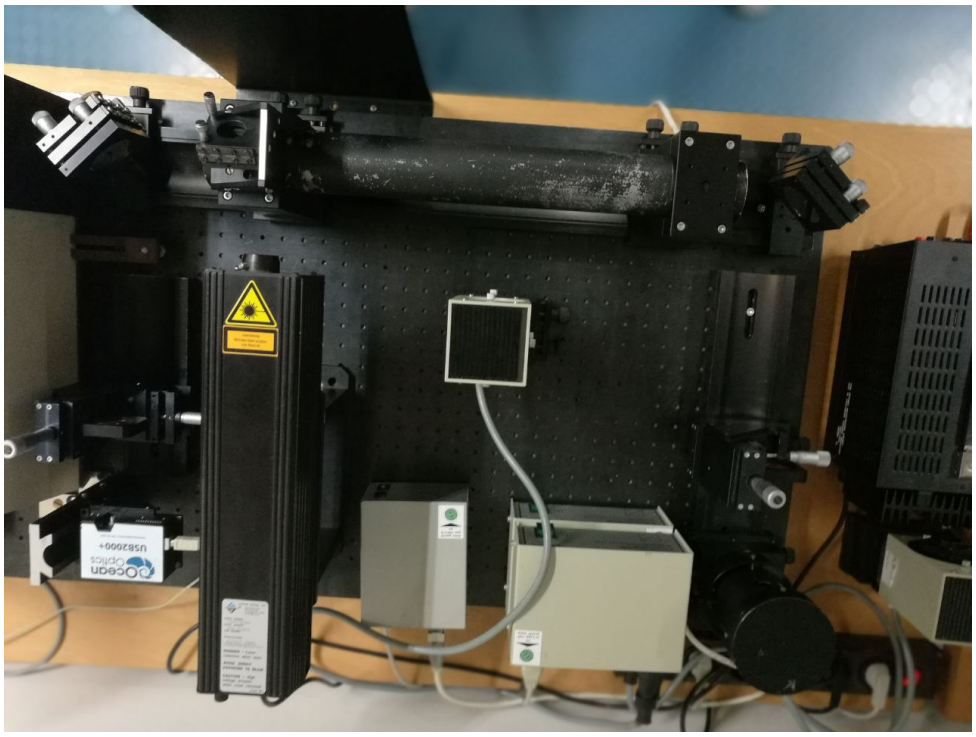

Figure 3.1.: Used experimental setup

# 4. Experimental procedure

## 4.1. Absorption

For the first part of our experiment the lenses and the mirrors were positioned in a way that one was able to clearly see the halogen tube of the used lamp on a piece of paper which was held in front of the spectrometer. Than, using the real-time data from the CCD-spectrometer, our setup was calibrated in a way that one obtained a maximized signal from our CCD. After the calibration measurement of the continuous spectrum of our lamp was made. In a next step, the iodine tube was installed in the setup. The tube had to be constantly heated using a hair dryer, otherwise the glass side, where the light was supposed to enter the tube, would be completely covered with crystallized iodine. The setup was then recalibrated for maximized intensity and the spectrum of the iodine was taken.

## 4.2. Emission

The first task in this part of the experiment consisted in calibrating the monochromator. Therefore the halogen lamp was first replaced by a mercury vapour lamp. Afterwards a small range of 2-3 nano metres were selected, where according to [Ver] a peak should be detected , for the monochromator to scan. Using that peak the signal strength was maximized by varying the range of the monochromator and varying the slit opening in front of the device. In our case we used a range of 100k for the discriminator and an opening of 35 $\mu$m for the spectrum of the mercury vapour lamp. Therefore the monochromator scanned the area from 4000-6000 Å with a rate of 2 $\text{Å}\,\text{s}^{-1}$.
For the next step the mercury vapour lamp was replaced by the He-Ne laser. The mirror on the iodine tube, on which the Laser was reflected into the tube, was configured in a way that the beam was travelling trough the tube. Additionally the laser point that hits the table after travelling through the tube has to be as sharp as possible.
At this point the room is supposed to be darkened as good as possible. A black blanket was used to cover the setup and all lights were turned of. Then one was supposed to configure the monochromator in a way that one could observe the peak of the laser at around 6330 Å. This was not possible to achieve. Unexpected behaviour on the monochromator has been observed, for example the registration of peaks by the monochromator even though the laser was turned off and no registration of peaks, even though it was turned on.
After consultation with the assistant, it was decided that it was not possible for us to get any useful data so it was decided that we should focus on the absorption part in the analysis.

# 5. Evaluation

The evaluation consists of two different sections. The first one contains the absorption of the iodine molecule, the second one is a short evaluation of the emission.

## 5.1. Absorption

### 5.1.1. Spectrum of the halogen lamp

First it was checked whether the halogen lamp emitted a continuous wavelength spectrum to be sure that during the measurements the only visible absorption bands originated from the iodine. In Figure 5.1 the relative intensity is plotted against the wavelength. As expected, there were no absorption bands.

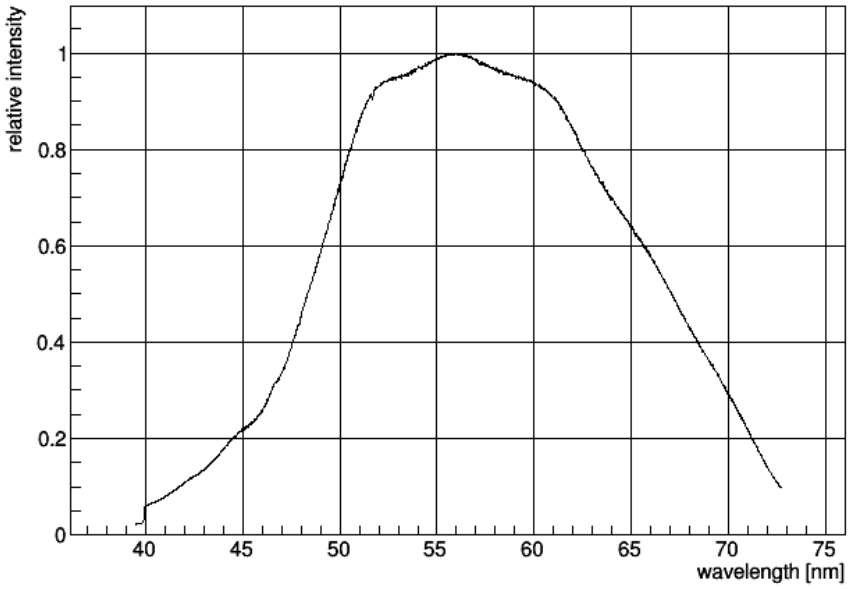


Figure 5.1.: Wavelength spectrum of the halogen lamp

### 5.1.2. Spectrum of the iodine

Then the iodine was put in. In Figure 5.2 the relative intensity is plotted over the wavelength. The next task is to determine the dips that belong to $n'' = 0$, $n'' = 1$ and to $n'' = 2$.

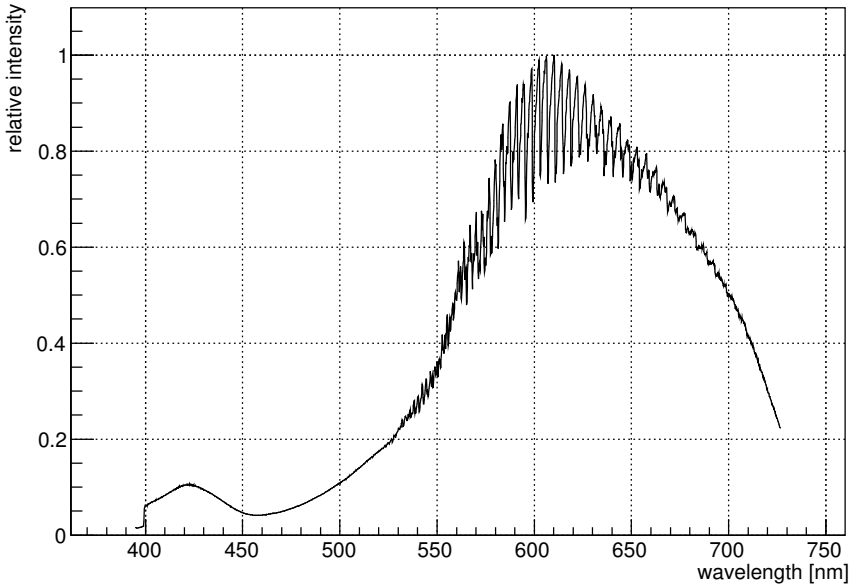


Figure 5.2.: Absorptionspectrum of the iodine

### 5.1.3. Identification of the vibronic bands

First the vibronic bands pertaining to $n'' = 0$ were looked at. Therefore the hint $n'' = 0 \rightarrow n' = 25 \Rightarrow \lambda = 545.8\,\text{nm}$ from the instruction was used. With the measured data the wavelength belonging to this transition was determined to $\lambda''(25) = 545.4\,\text{nm}$ which compatible with the spectral resolution of 0.4 nm. With this help and the Frank-Condon-Principle seven to twelve dips belonging to the different progressions were found. They are marked in Figure 5.3 with a vertical line. For $n'' = 1$ the first point was taken close from the same starting point but showed a dip that did not belong to the progression $n'' = 0$ (see Figure 5.4). The same procedure was used for $n'' = 2$ (see Figure 5.5).

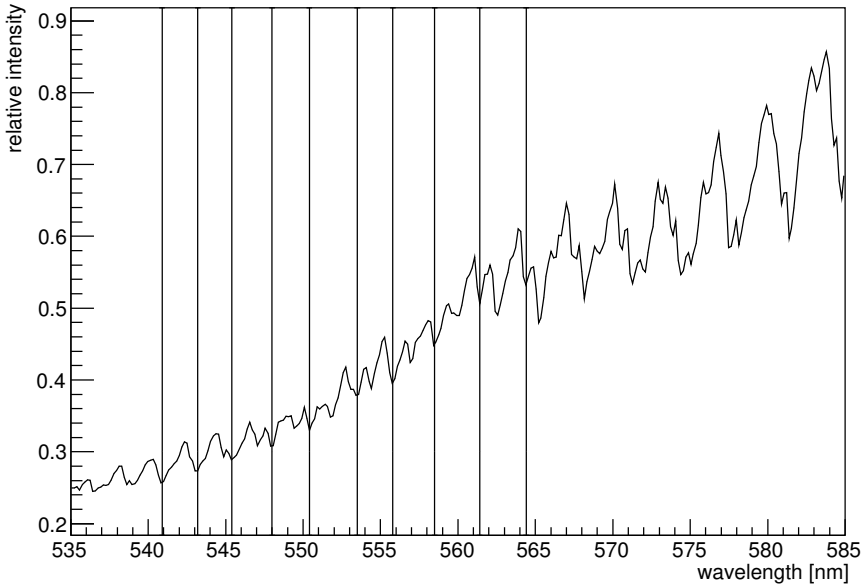


Figure 5.3.: Dips belonging to the progression $n'' = 0$

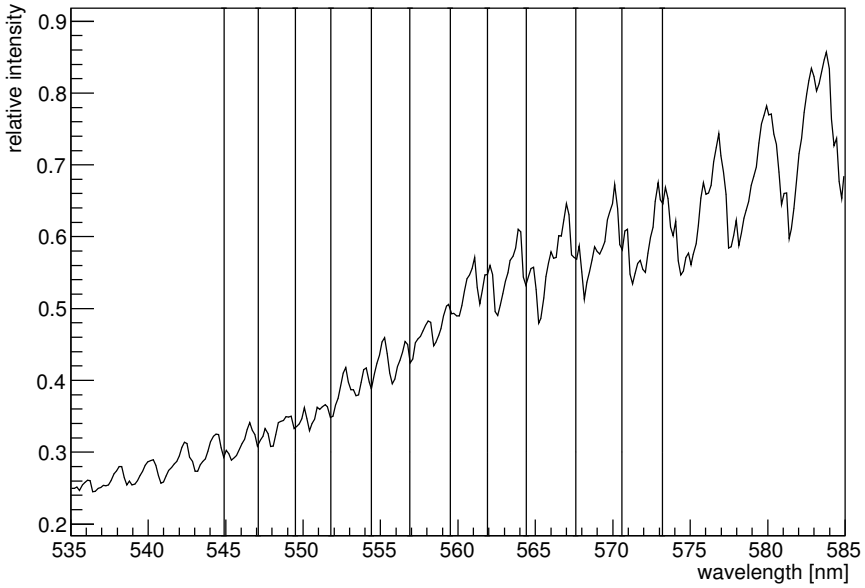


Figure 5.4.: Dips belonging to the progression $n'' = 1$

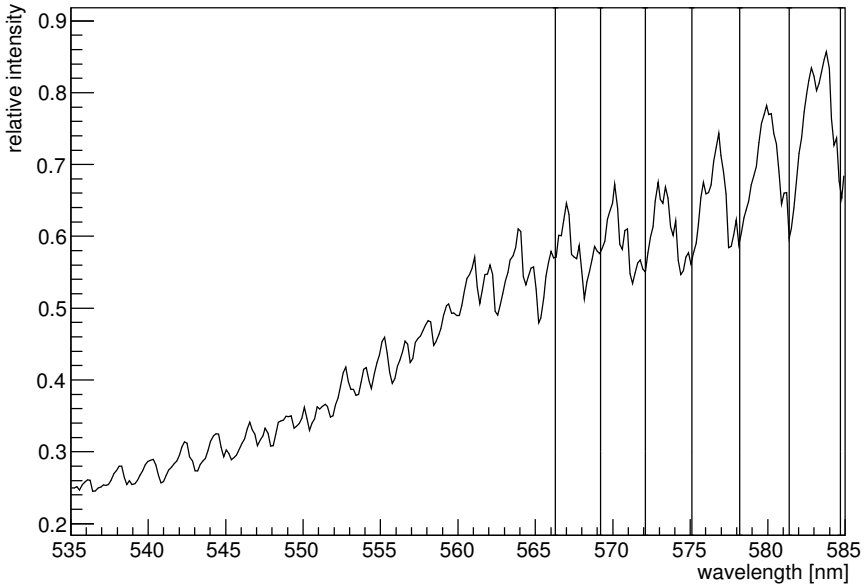


Figure 5.5.: Dips belonging to the progression $n'' = 2$

### 5.1.4. Birge-Sponer-Plot

Next the Birge-Sponer-Plot was drawn. The conversion of the wavelength in air to the one in vacuum was neglected because firstly the influence of the wavelength's uncertainty, which is about $s_\lambda = 0.2\,\text{nm}$ for $n'' = 0, 1$ and $s_\lambda = 0.1\,\text{nm}$ for $n'' = 2$, was estimated high enough. The uncertainties were determined differently because the dips for $n'' = 2$ were much sharper and easier to recognize. Additionally there are only four refractive indexes given for four different wavelengths, thus the correction for each point would not even be accurate.
The energy difference $\Delta G$ is given by

$$\Delta G(n' + 1/2) = G(n' + 1) - G(n') = \frac{1}{\lambda(n' + 1)} - \frac{1}{\lambda(n')} \equiv \sigma(n' + 1) - \sigma(n') \tag{5.1}$$

$$s_{\Delta G(n'+1/2)} = \sqrt{s^2_{\sigma(n'+1)} + s^2_{\sigma(n')}} \tag{5.2}$$

The determined values can be seen in the appendix, Tables A.1, A.2, A.3. A fit test of the form

$$f\left(n' + \frac{1}{2}\right) = a - b \cdot (2 \cdot n' + 2) \tag{5.3}$$

was applied to the data, with $a \equiv \omega'_e$, $b \equiv x'_e\omega'_e$. The Birge-Sponer-Plot, which consist of $\Delta G$ being plotted over $n' + 1/2$, and the fit are shown in Figures 5.6, 5.7, 5.8.

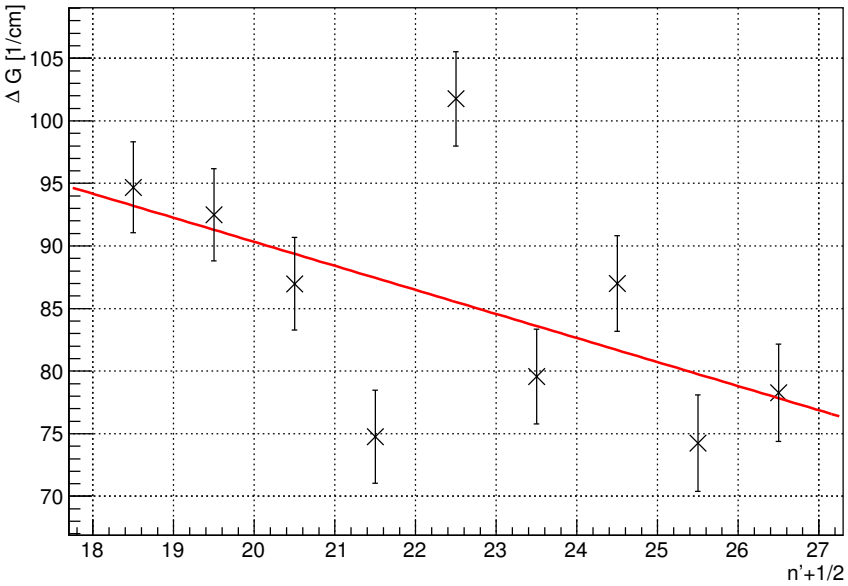


Figure 5.6.: Birge-Sponer-Plot for the progression $n'' = 0$

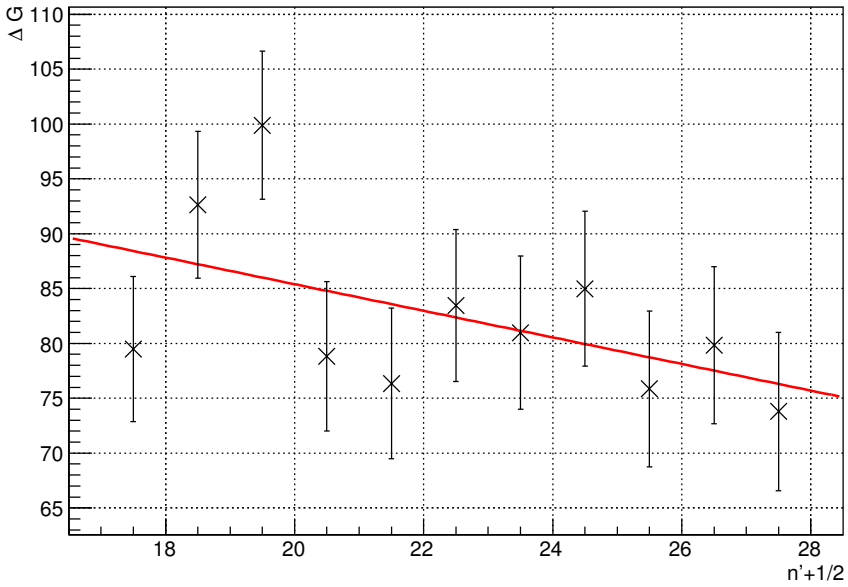


Figure 5.7.: Birge-Sponer-Plot for the progression $n'' = 1$

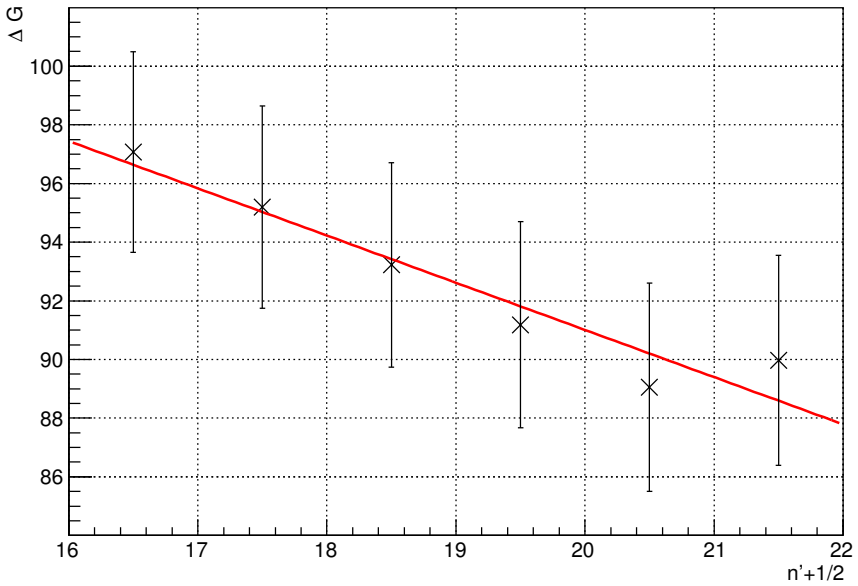


Figure 5.8.: Birge-Sponer-Plot for the progression $n'' = 2$

The fit results and the literature values taken from [BI, p. 51] are shown in Table 5.1.

Table 5.1.: Fit results of the Birge-Sponer-Plot for the progression $n'' = 0, 1, 2$

| | $\omega'_e$ | $\omega'_e x'_e$ | $\chi$/NoF |
|---|---|---|---|
| $n'' = 0$ | $126 \pm 26\,\mathrm{cm}^{-1}$ | $0.9 \pm 0.5\,\mathrm{cm}^{-1}$ | 1.68 |
| $n'' = 1$ | $111 \pm 15\,\mathrm{cm}^{-1}$ | $0.6 \pm 0.3\,\mathrm{cm}^{-1}$ | 1.05 |
| $n'' = 2$ | $125 \pm 17\,\mathrm{cm}^{-1}$ | $0.8 \pm 0.4\,\mathrm{cm}^{-1}$ | 0.076 |
| lit | $125.3 \pm 0.1\,\mathrm{cm}^{-1}$ | $0.70 \pm 0.01\,\mathrm{cm}^{-1}$ | |

Both of the literature values are in the uncertainty area of the fitted values, but the uncertainties are very big. Their origin can be placed in the amount of data taken which is very small with only seven to twelve points.

### 5.1.5. Identification of the dissociation energy of the $B^3\Pi_u^+$

There are two different ways to determine the dissociation energy which is given from [BI, p. 55] as $D_{e,lit} = 4391\,\mathrm{cm}^{-1}$.

**Approximation with Morse potential:**

With (2.6) the dissociation energy is calculated by using

$$D_e = \frac{\omega_e'^2}{4\omega'_e x'_e} \tag{5.4}$$

$$s_{D_e} = D_e \cdot \sqrt{\left(\frac{2 \cdot s_{\omega'_e}}{\omega'_e}\right)^2 + \left(\frac{s_{\omega'_e x'_e}}{\omega'_e x'_e}\right)^2} \tag{5.5}$$

which yields

$$n'' = 0: \qquad D_e = 4400 \pm 3000\,\mathrm{cm}^{-1} \tag{5.6}$$
$$n'' = 1: \qquad D_e = 5100 \pm 2900\,\mathrm{cm}^{-1} \tag{5.7}$$
$$n'' = 2: \qquad D_e = 4900 \pm 2900\,\mathrm{cm}^{-1} \tag{5.8}$$

The literature value is in the confidence area of the measured value. This is induced by the high uncertainty of the fitted parameters.

**Ascertainment by using the energy differences**

As it is written in the theoretical foundations the dissociation energy can be calculated by summing up all of the energy differences. This method can not be used because of the lack of data for low and high vibronic states. But it can be achieved by integration over the area that is given by the line of the fit and the intersection with the y- and x-axis

$$D_e = \int_0^{n'_{diss}} \Delta G(n' + 1/2) dn' \tag{5.9}$$

where $n'_{diss}$ is the integer value of the intersection with the x-axis determined by

$$\Delta G(n'_{diss} + 1/2) = \omega'_e - \omega'_e x'_e \cdot (2 \cdot n'_{diss} + 2) \stackrel{!}{=} 0 \tag{5.10}$$
$$\Leftrightarrow n'_{diss} = \frac{\omega'_e}{2 \cdot \omega'_e x'_e} - 1 \tag{5.11}$$
$$s_{n'_{diss}} = \sqrt{\left(\frac{s_{\omega'_e}}{2 \cdot \omega'_e x'_e}\right)^2 + \left(\frac{\omega'_e}{2 \cdot (\omega'_e x'_e)^2} \cdot s_{\omega'_e x'_e}\right)^2} \tag{5.12}$$

This yields

$$n'' = 0: \qquad n'_{diss} = 70 \pm 40 \tag{5.13}$$
$$n'' = 1: \qquad n'_{diss} = 93 \pm 48 \tag{5.14}$$
$$n'' = 2: \qquad n'_{diss} = 78 \pm 40 \tag{5.15}$$

Therefrom the intersection with the x- and y-axis are known and the area of the triangular can be computed using

$$D_e = \frac{1}{2} \cdot n'_{diss} \cdot \omega'_e \tag{5.16}$$
$$s_{D_e} = D_e \cdot \sqrt{\left(\frac{s_{n'_e}}{n'_e}\right)^2 + \left(\frac{s_{\omega'_e}}{\omega'_e}\right)^2} \tag{5.17}$$

This results dissociation energies of

$$n'' = 0: \qquad D_e = 4400 \pm 2700\,\mathrm{cm}^{-1} \tag{5.18}$$
$$n'' = 1: \qquad D_e = 5200 \pm 2800\,\mathrm{cm}^{-1} \tag{5.19}$$
$$n'' = 2: \qquad D_e = 4900 \pm 2600\,\mathrm{cm}^{-1} \tag{5.20}$$

whose confidence interval includes the literature value again because of the magnitude of the uncertainty.

### 5.1.6. Determination of the excitation energy $T_e'$

Before the energy of the state $n'' = 0$

$$G''(n) = \omega_e'' \left(n + \frac{1}{2}\right) - \omega_e'' x_e'' \left(n + \frac{1}{2}\right)^2 \tag{5.21}$$

$$G''(0) = \frac{1}{2}\omega''_e - \frac{1}{4}\omega_e'' x_e'' \tag{5.22}$$

can be determined it is necessary to ascertain $\omega_e''$ and $\omega_e'' x_e''$. You can get these parameters by looking at the differences

$$\Delta G''\left(\frac{1}{2}\right) = G''(1) - G''(0) = \omega_e'' - 2 \cdot \omega_e'' x_e'' \tag{5.23}$$

$$\Delta G''\left(\frac{3}{2}\right) = G''(2) - G''(1) = \omega_e'' - 4 \cdot \omega_e'' x_e'' \tag{5.24}$$

and subtract (5.24) from them first once and then twice (5.23)

$$2 \cdot \Delta G''(\frac{1}{2}) - \Delta G''(\frac{3}{2}) = \omega_e'' \tag{5.25}$$

$$\Delta G''(\frac{1}{2}) - \Delta G''(\frac{3}{2}) = 2 \cdot \omega_e'' x_e'' \tag{5.26}$$

$$\Rightarrow G''(0) = \frac{7}{8}\Delta G''\left(\frac{1}{2}\right) - \frac{3}{8}\Delta G''\left(\frac{3}{2}\right) \tag{5.27}$$

Because of the relations

$$\Delta G''\left(\frac{1}{2}\right) = \sigma_{n''=0}(n') - \sigma_{n''=1}(n') \tag{5.28}$$

$$\Delta G''\left(\frac{3}{2}\right) = \sigma_{n''=1}(n') - \sigma_{n''=2}(n') \tag{5.29}$$

the differences can be calculated. To estimate $\Delta G\left(\frac{1}{2}\right)$ the average of $\sigma_{n''=1,n''=0}(n')$ with $n' \in [19, 27]$ and for $\Delta G\left(\frac{3}{2}\right)$ the average of $\sigma_{n''=2,n''=1}(n')$ with $n' \in [17, 22]$ were used. This yields

$$G''(0) = 95 \pm 7\,\mathrm{cm}^{-1} \tag{5.30}$$

for the energy of the state $n'' = 0$. Now there are no unknown parameters in the equation

$$T_e' = \sigma_{n''=0}(n') + G''(0) - n \cdot \left(\frac{\Delta G_{n''=0}\left(\frac{1}{2}\right) + \Delta G_{n''=0}\left(n' + \frac{1}{2}\right)}{2}\right) \tag{5.31}$$

if $n'$ is chosen from one of the found vibronic states of the progression of $n'' = 0$. With $n' = 20$ follows $\sigma_{n''=0}(20) = 17\,905 \pm 3\,\mathrm{cm}^{-1}$, $\Delta G_{n''=0}\left(20 + \frac{1}{2}\right) = 87 \pm 7\,\mathrm{cm}^{-1}$ and $\Delta G_{n''=0}\left(\frac{1}{2}\right) = 126 \pm 26\,\mathrm{cm}^{-1}$ and for the excitation energy

$$T_e' = 15\,900 \pm 300\,\mathrm{cm}^{-1} \tag{5.32}$$

where the uncertainties from $\sigma$ and $G''(0)$ were neglected because the last term dominates. Thus the literature value of $T_e' = 15\,770.59\,\mathrm{cm}^{-1}$ is situated in the simple uncertainty area the measured value.

### 5.1.7. Ascertainment of $E_{diss}$

From [Mey, p. 23] $E_{diss}$ is calculated by

$$E_{diss} = T'_e - G''(0) + D'_e \tag{5.33}$$

$$s_{E_{diss}} = \sqrt{s^2_{T'_e} + s^2_{G''(0)} + s^2_{D'_e}} \tag{5.34}$$

$$\Rightarrow E_{diss} = 20\,200 \pm 2700\,\mathrm{cm}^{-1} \tag{5.35}$$

and the approximate value from [BI, p. 57] lays with $E_{diss} \approx 20\,000\,\mathrm{cm}^{-1}$ in the uncertainty area of the calculated value.

### 5.1.8. Morse potential

Last the Morse potential is to be estimated. Therefore it is necessary to compute the missing parameters $a$ and $r_e$. With (2.5) follows [1]

$$a = \sqrt{\omega'_e x'_e \cdot \frac{4\pi c \mu}{\hbar}} \tag{5.36}$$

$$s_a = \sqrt{\frac{\pi \cdot c \cdot \mu}{\hbar \cdot \omega'_e x'_e}} \cdot s_{\omega'_e x'_e} \tag{5.37}$$

$$\Rightarrow a = 1.7 \pm 0.4\,\text{Å}^{-1} \tag{5.38}$$

$$\overset{\text{lit. val.}}{\Rightarrow} a = 1.62\,\text{Å}^{-1} \tag{5.39}$$

and with the theoretical value of the rotation constant $B'_e = 0.029\,\mathrm{cm}^{-1}$

$$r_e = \sqrt{\frac{\hbar}{4\pi \cdot c \cdot \mu \cdot} B'_e} = 3.02\,\text{Å} \tag{5.40}$$

[1] $c = 3 \times 10^{10}\,\mathrm{cm\,s}^{-1}$
$\mu = 1.05 \times 10^{-22}\,\mathrm{g}$
$\hbar = 1.05 \times 10^{-27}\,\mathrm{g\,cm^2\,s}^{-1}$

Both of the Morse potentials are plotted in Figure 5.9. The dashed line represents the calculated potential with the literature values and the continuous line with the measured values. Uncertainties are not drawn because only the trend of both lines is observed.

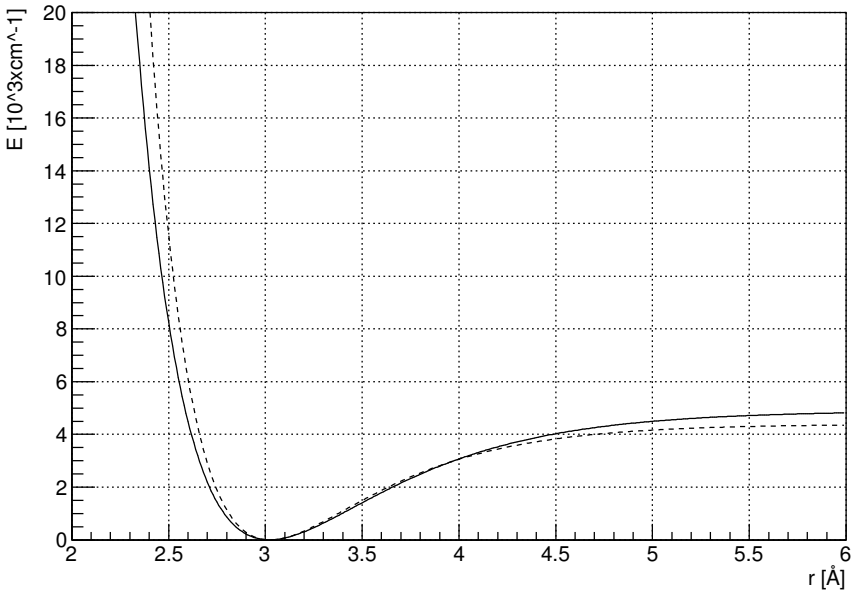


Figure 5.9.: Comparison of the calculated Morse potentials with measured and literature values

It can be seen that the estimated potential goes along with the theoretic one.

## 5.2. Emission

The evaluation of the emission spectrum consists of two tasks, firstly the calibration of the monochromator and secondly the recording of the emission spectrum.

### 5.2.1. Calibration of the monochromator

For wavelengths in the area of $\lambda = \left[4000\,\text{Å}, 6000\,\text{Å}\right]$ the monochromator was calibrated by using a mercury lamp which sharp spectral lines were given in [VER, p. 6] and compared with the measured spectral lines in Table 5.2 where the uncertainty belonging to the measured value was estimated to $s_\lambda = 0.1\,\text{nm}$. The recorded spectrum was plotted against the wavelength as it can be seen in Figure 5.10.

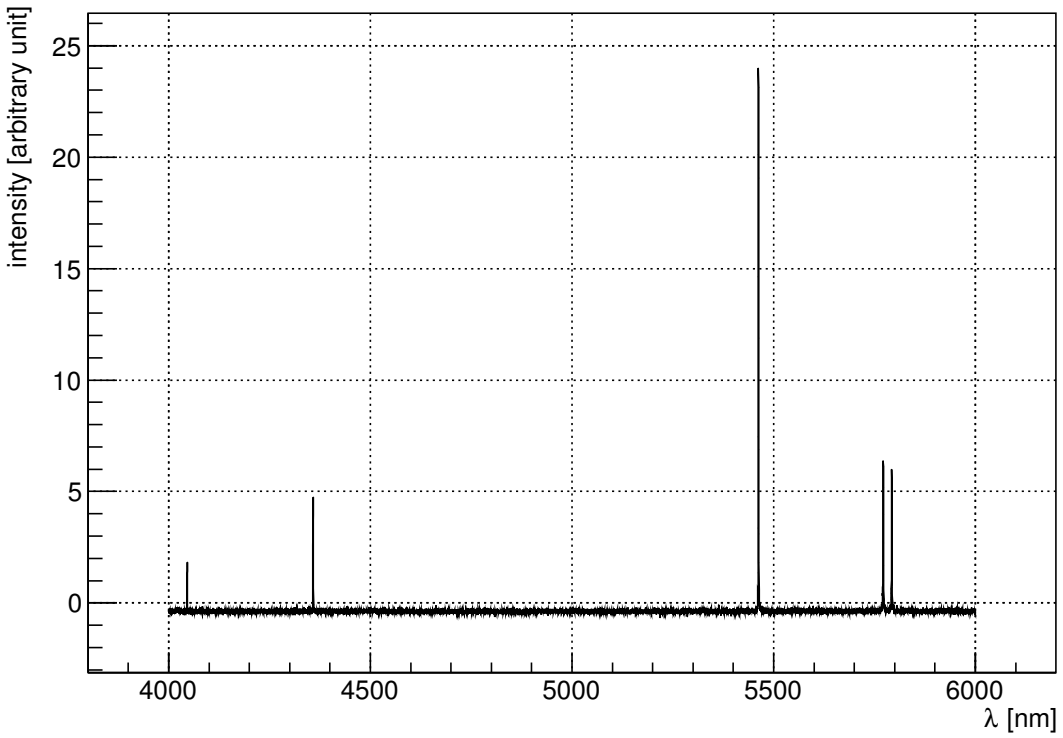


Figure 5.10.: Spectral lines of the Hg-lamp

Table 5.2.: Comparison of the literature and measured spectral lines of the Hg-lamp

| $\lambda_{\text{lit}}$ | $\lambda_{\text{measured}}$ |
|---|---|
| 404.7 nm | $404.6 \pm 0.1$ nm |
| 435.8 nm | $435.8 \pm 0.1$ nm |
| 546.1 nm | $546.2 \pm 0.1$ nm |
| 577.0 nm | $577.1 \pm 0.1$ nm |
| 579.1 nm | $579.3 \pm 0.1$ nm |

All literature values except the last one are in $1\sigma$ and the last one is in $2\sigma$ level of confidence. Thus the monochromator was calibrated correctly.

### 5.2.2. Recording of the emission spectrum

Next the emission spectrum of the iodine should have been analysed. In this experimentation it was not possible to get reasonable peaks to the resonance frequency of the used laser. The detected peaks were rather randomly appearing signals exemplary shown in Figure 5.11. Hence the emission spectrum could not be detected.

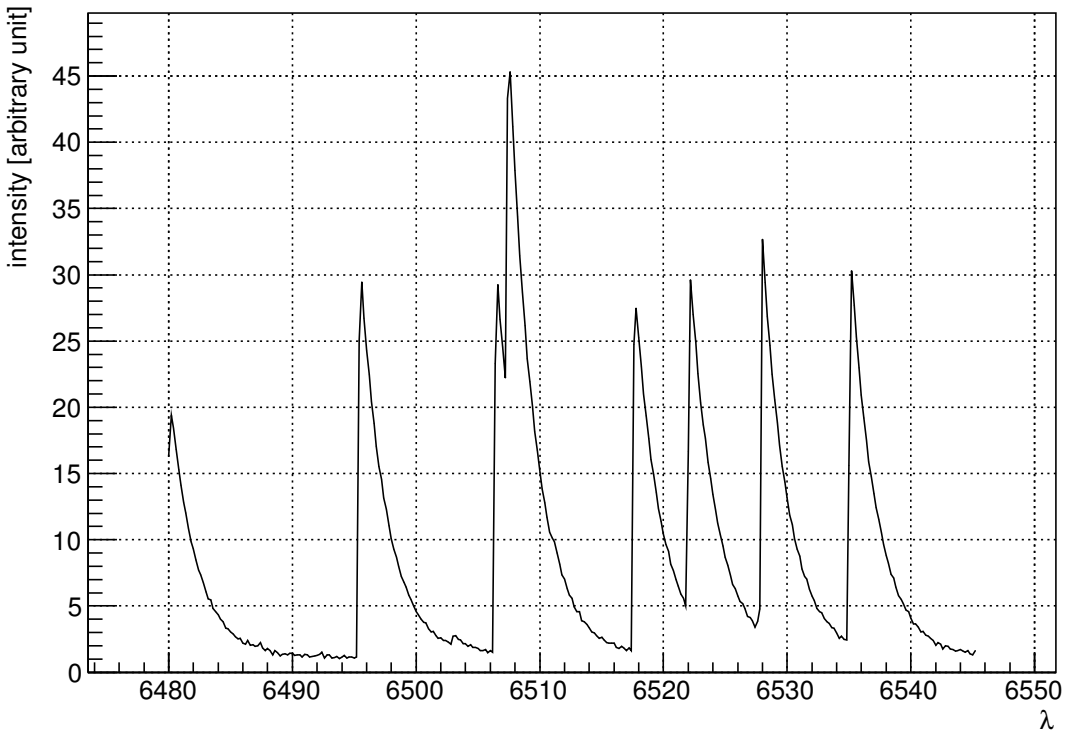


Figure 5.11.: Randomly appearing peaks detected during searching the maximum at the area of the resonance frequency

# 6. Error Discussion

## 6.1. Absorption

For the analysis of the absorption spectrum, the used wavelengths were determined by hand and have therefore a reading error. However one can see, that in order to get a realistic reduced $\chi^2$ one had to choose unrealistically small reading errors. For example in n" = 2 we already fixed a reading error of 0.1 nm and we still get a reduced $\chi^2$ which is far under 1. This happened because our measurement shows such a highly linear course in a small amount of close points. One could describe our measurement as a statistical anomaly because it is not common that values show such a linear behaviour when they are determined by hand.
This lack of data causes extremely high uncertainties to all of the fit parameters, hence the estimated values including these parameters get high uncertainties as well. Accordingly the uncertainties could have been reduced by identifying more dips in the graphs but as this was not possible, the only way to reduce the errors would have been rating the uncertainties differently. Especially in Table 5.1 it's obvious that the determined parameters have a much higher precision than the error suggests.
Nearly all of the calculated values used at least one of the fitted parameters, thus the high uncertainties could only have been prevented by choosing smaller ones. But as we did not know which uncertainties were reasonable, the calculations were done with the errors given by the fit.

## 6.2. Emission

For the emission part of the experiment, it was not possible for us to get a significant signal using the He-Ne laser. Even though we constantly heated the iodine using the hair dryer, it could be that there was not enough gas in the iodine tube for the laser to be reflected on and deviated toward the monochromater.
In addition to that our instruments registered activity even when the laser was off and did not register activity when the laser was turned on, so one could also guess that the electronics of the monochromator was malfunctioning because it overheated under the heated black blanket. It's possible that the measured peaks go along with earlier detected random peaks that belonged to the light in the room. Maybe some sunlight came in and led to these peaks. If the grid is made out of a material which expands rapidly when heated, it became big enough to accept infrared light.

# 7. Summary

## 7.1. Absorption

In the first part of the experiment, all the measured values are matching their literature values in a single standard deviation margin.
For the Birge-Sponer plot we obtain the results that are shown in Table 7.1.

Table 7.1.: Results Birge-Sponer-Plot

| | $\omega'_e$ | $\omega'_e x'_e$ | $\chi$/NoF |
|---|---|---|---|
| $n'' = 0$ | $126 \pm 26\,\mathrm{cm}^{-1}$ | $0.9 \pm 0.5\,\mathrm{cm}^{-1}$ | 1.68 |
| $n'' = 1$ | $111 \pm 15\,\mathrm{cm}^{-1}$ | $0.6 \pm 0.3\,\mathrm{cm}^{-1}$ | 1.05 |
| $n'' = 2$ | $125 \pm 17\,\mathrm{cm}^{-1}$ | $0.8 \pm 0.4\,\mathrm{cm}^{-1}$ | 0.076 |
| lit | $125.3 \pm 0.1\,\mathrm{cm}^{-1}$ | $0.70 \pm 0.01\,\mathrm{cm}^{-1}$ | |

The dissociation energy was calculated in two different ways. In Table 7.2 it can be seen, that the approximation of the Morse potential yielded nearly the same results as the correct estimation by using the Birge-Sponer-Plot.

Table 7.2.: Results of the dissociation energy

| $n''$ | $D_{e,morse}$ | $D_e$ |
|---|---|---|
| 0 | $4400 \pm 3000\,\mathrm{cm}^{-1}$ | $4400 \pm 2700\,\mathrm{cm}^{-1}$ |
| 1 | $5200 \pm 2900\,\mathrm{cm}^{-1}$ | $5200 \pm 2800\,\mathrm{cm}^{-1}$ |
| 2 | $4900 \pm 2900\,\mathrm{cm}^{-1}$ | $4900 \pm 2600\,\mathrm{cm}^{-1}$ |

The literature value as taken from [BI, p. 55] is $D_{e,lit} = 4391\,\mathrm{cm}^{-1}$ and compliant to all measured values.
Using our calculated values, we obtain an excitation energy $T'_e$ of $15\,900 \pm 300\,\mathrm{cm}^{-1}$. However the literature value is given by $15\,770.59\,\mathrm{cm}^{-1}$ which is compatible with the measured value.
Lastly we obtained $E_{diss} = 19\,700 \pm 2600\,\mathrm{cm}^{-1}$ as compared to a literature value of $20\,000\,\mathrm{cm}^{-1}$.
Using the measured values the Morse potential was agreeable with the Morse potential we calculated with the literature values.

## 7.2. Emission

For this part of the experiment, we measured the emission spectrum of a mercury vapour lamp. The result can be seen in in 5.10. The spectral lines were reconcilable with the literature values. We were not able to perform any other measurements for the emission spectrum for the reasons that were discussed in point 6 of our report.

# Bibliography

[Mey] Meyer, Martine, *Verbesserung des Versuchs Spektroskopie am J 2 - Molekül des Fortgeschrittenen Praktikums*, Wissenschaftliche Arbeit für das Staatsexamen im Fach Physik. Universität Freiburg, 17. Oktober 2014.

[BI] Bitsch, Klaus, *Aufbau des Versuchs Spektroskopie am J 2 - Molekül*, Staatsexamensarbeit. Universität Freiburg, Februar 1977.

[Ver] *Versuchsanleitung, Fortgeschrittenen Praktikum Teil 1, Spektroskopie am Iod Molekül*, Universität Freiburg, 1. Oktober 2014.

# A. Tables

Table A.1.: $n'' = 0$ progression, data for Birge-Sponer-Plot

| $n'$ | $\lambda(n')$ | $\sigma(n')$ | $\Delta G(n' + 1/2)$ |
|---|---|---|---|
| 27.0 | $540.9 \pm 0.2\,\mathrm{nm}$ | $18\,488 \pm 7\,\mathrm{cm}^{-1}$ | |
| 26.0 | $543.2 \pm 0.2\,\mathrm{nm}$ | $18\,409 \pm 7\,\mathrm{cm}^{-1}$ | $78 \pm 7\,\mathrm{cm}^{-1}$ |
| 25.0 | $545.4 \pm 0.2\,\mathrm{nm}$ | $18\,335 \pm 7\,\mathrm{cm}^{-1}$ | $74 \pm 7\,\mathrm{cm}^{-1}$ |
| 24.0 | $548.0 \pm 0.2\,\mathrm{nm}$ | $18\,248 \pm 7\,\mathrm{cm}^{-1}$ | $87 \pm 7\,\mathrm{cm}^{-1}$ |
| 23.0 | $550.4 \pm 0.2\,\mathrm{nm}$ | $18\,169 \pm 7\,\mathrm{cm}^{-1}$ | $80 \pm 7\,\mathrm{cm}^{-1}$ |
| 22.0 | $553.5 \pm 0.2\,\mathrm{nm}$ | $18\,067 \pm 7\,\mathrm{cm}^{-1}$ | $102 \pm 7\,\mathrm{cm}^{-1}$ |
| 21.0 | $555.8 \pm 0.2\,\mathrm{nm}$ | $17\,992 \pm 6\,\mathrm{cm}^{-1}$ | $75 \pm 7\,\mathrm{cm}^{-1}$ |
| 20.0 | $558.5 \pm 0.2\,\mathrm{nm}$ | $17\,905 \pm 6\,\mathrm{cm}^{-1}$ | $87 \pm 7\,\mathrm{cm}^{-1}$ |
| 19.0 | $561.4 \pm 0.2\,\mathrm{nm}$ | $17\,813 \pm 6\,\mathrm{cm}^{-1}$ | $92 \pm 7\,\mathrm{cm}^{-1}$ |

Table A.2.: $n'' = 1$ progression, data for Birge-Sponer-Plot

| $n'$ | $\lambda(n')$ | $\sigma(n')$ | $\Delta G(n' + 1/2)$ |
|---|---|---|---|
| 28.0 | $544.9 \pm 0.2\,\mathrm{nm}$ | $18\,352 \pm 7\,\mathrm{cm}^{-1}$ | |
| 27.0 | $547.1 \pm 0.2\,\mathrm{nm}$ | $18\,278 \pm 7\,\mathrm{cm}^{-1}$ | $74 \pm 7\,\mathrm{cm}^{-1}$ |
| 26.0 | $549.5 \pm 0.2\,\mathrm{nm}$ | $18\,198 \pm 7\,\mathrm{cm}^{-1}$ | $80 \pm 7\,\mathrm{cm}^{-1}$ |
| 25.0 | $551.8 \pm 0.2\,\mathrm{nm}$ | $18\,123 \pm 7\,\mathrm{cm}^{-1}$ | $76 \pm 7\,\mathrm{cm}^{-1}$ |
| 24.0 | $554.4 \pm 0.2\,\mathrm{nm}$ | $18\,038 \pm 7\,\mathrm{cm}^{-1}$ | $85 \pm 7\,\mathrm{cm}^{-1}$ |
| 23.0 | $556.9 \pm 0.2\,\mathrm{nm}$ | $17\,957 \pm 6\,\mathrm{cm}^{-1}$ | $81 \pm 7\,\mathrm{cm}^{-1}$ |
| 22.0 | $559.5 \pm 0.2\,\mathrm{nm}$ | $17\,873 \pm 6\,\mathrm{cm}^{-1}$ | $83 \pm 7\,\mathrm{cm}^{-1}$ |
| 21.0 | $561.9 \pm 0.2\,\mathrm{nm}$ | $17\,797 \pm 6\,\mathrm{cm}^{-1}$ | $76 \pm 7\,\mathrm{cm}^{-1}$ |
| 20.0 | $564.4 \pm 0.2\,\mathrm{nm}$ | $17\,718 \pm 6\,\mathrm{cm}^{-1}$ | $79 \pm 7\,\mathrm{cm}^{-1}$ |
| 19.0 | $567.6 \pm 0.2\,\mathrm{nm}$ | $17\,618 \pm 6\,\mathrm{cm}^{-1}$ | $100 \pm 7\,\mathrm{cm}^{-1}$ |
| 18.0 | $570.6 \pm 0.2\,\mathrm{nm}$ | $17\,525 \pm 6\,\mathrm{cm}^{-1}$ | $93 \pm 7\,\mathrm{cm}^{-1}$ |
| 17.0 | $573.2 \pm 0.2\,\mathrm{nm}$ | $17\,446 \pm 6\,\mathrm{cm}^{-1}$ | $79 \pm 7\,\mathrm{cm}^{-1}$ |

Table A.3.: $n'' = 2$ progression, data for Birge-Sponer-Plot

| $n'$ | $\lambda(n')$ | $\sigma(n')$ | $\Delta G(n' + 1/2)$ |
|---|---|---|---|
| 22.0 | $566.3 \pm 0.1\,\mathrm{nm}$ | $17\,658 \pm 3\,\mathrm{cm}^{-1}$ | |
| 21.0 | $569.2 \pm 0.1\,\mathrm{nm}$ | $17\,569 \pm 3\,\mathrm{cm}^{-1}$ | $90 \pm 4\,\mathrm{cm}^{-1}$ |
| 20.0 | $572.1 \pm 0.1\,\mathrm{nm}$ | $17\,479 \pm 3\,\mathrm{cm}^{-1}$ | $89 \pm 4\,\mathrm{cm}^{-1}$ |
| 19.0 | $575.1 \pm 0.1\,\mathrm{nm}$ | $17\,388 \pm 3\,\mathrm{cm}^{-1}$ | $91 \pm 4\,\mathrm{cm}^{-1}$ |
| 18.0 | $578.2 \pm 0.1\,\mathrm{nm}$ | $17\,295 \pm 3\,\mathrm{cm}^{-1}$ | $93 \pm 3\,\mathrm{cm}^{-1}$ |
| 17.0 | $581.4 \pm 0.1\,\mathrm{nm}$ | $17\,200 \pm 3\,\mathrm{cm}^{-1}$ | $95 \pm 3\,\mathrm{cm}^{-1}$ |
| 16.0 | $584.7 \pm 0.1\,\mathrm{nm}$ | $17\,103 \pm 3\,\mathrm{cm}^{-1}$ | $97 \pm 3\,\mathrm{cm}^{-1}$ |